*Antarctic Science 12 (4): 477–491 (2000)* © British Antarctic Survey Printed in the United Kingdom

# Eocene and Oligocene volcanism at Mount Petras, Marie Byrd Land: implications for middle Cenozoic ice sheet reconstructions in West Antarctica

T.I. WILCH[1] AND W.C. McINTOSH[2]

[1]*Department of Geological Sciences, Albion College, Albion, MI 49224, USA*
[2]*Department of Earth and Environmental Science, New Mexico Tech, Socorro, NM 87801, USA*

**Abstract:** Evidence for one late Eocene and four middle Oligocene eruptions of Mount Petras, Marie Byrd Land provides new insights into reconstructions of middle Tertiary ice sheet configurations, surface topography, and volcanism in West Antarctica. The interpretation presented here of the volcanic record at Mount Petras, based on detailed analyses of lithofacies, petrography, $^{40}Ar/^{39}Ar$ geochronology, and geochemistry, is significantly different from previous interpretations based on reconnaissance studies. A massive, 25 m thick, mugearite lava near the summit of Mount Petras is $^{40}Ar/^{39}Ar$ dated to 36.11 ± 0.22 Ma (2 σ uncertainty), indicating an onset of Cenozoic alkaline volcanism in the Marie Byrd Land Volcanic Province in latest Eocene time. Middle Oligocene (29–27 Ma) hawaiite volcaniclastic lithofacies at Mount Petras are interpreted as products of mixed magmatic (Strombolian style) and phreatomagmatic (Surtseyan style) subaerial eruptions. The four hawaiite outcrop areas exhibit characteristics of near-vent tuff cone environments. The near-vent deposits are located at different elevations and positions on Mount Petras and suggest four separate eruptive centres, with eruptions dated to between 28.59 ± 0.22 Ma and 27.18 ± 0.23 Ma. The mixed Surtseyan and Strombolian eruptions imply local or intermittent contact with external water, which we infer was derived from melting of a thin, local ice cap or ice and snow on slopes. The 29–27 Ma volcanic deposits at Mount Petras provide the oldest terrestrial evidence for glacial ice in Marie Byrd Land. The 29–27 Ma tuff cone deposits overlie an erosional unconformity, with > 400 m of topographic relief. The relatively high relief pre-volcanic environment is suggestive of ongoing erosion and is inconsistent with previous interpretations of a regional, low relief, early Cenozoic West Antarctic Erosion Surface.

Received 8 July 1999, accepted 10 May 2000

**Key words:** $^{40}Ar/^{39}Ar$ geochronology, Antarctica, glacial history, Marie Byrd Land, Surtseyan, volcaniclastic lithofacies, West Antarctic ice sheet

## Introduction

The mid-Cenozoic volcanic history at Mount Petras (75°51'S, 128°38'W), coastal Marie Byrd Land is critical for interpretations of inception of Cenozoic alkaline volcanism in Marie Byrd Land, early history of the West Antarctic ice sheet, and surface uplift of the Marie Byrd Land volcanic highlands (Fig. 1) (LeMasurier 1972a, 1972b, 1990a, LeMasurier & Rex 1982, 1983, LeMasurier *et al.* 1981, 1994). Mount Petras is a basement nunatak capped by the oldest known alkaline volcanic rocks in Marie Byrd Land, which have been K/Ar dated to *c.* 22–25 Ma (LeMasurier 1990a). The volcanic rocks were previously interpreted as subglacial hyaloclastite erosional remnants of a volcanic table mountain and cited as the first evidence of a thick regional ice sheet in West Antarctica (LeMasurier *et al.* 1981). The volcanic rocks crop out at the summit region of Mount Petras, where they overlie a bedrock unconformity situated at roughly 2700 m a.s.l. (LeMasurier *et al.* 1981). Similar pre-volcanic erosion surfaces in Marie Byrd Land are situated at progressively lower elevations and capped by progressively younger volcanic rocks away from Mount Petras (LeMasurier & Rex 1983). LeMasurier & Landis (1996) suggested that these remnant surfaces represent relicts of a former regional erosion surface, termed the West Antarctic Erosion Surface (WAES), which was postulated to have formed by continent-wide early Cenozoic marine peneplanation. The elevation differences of these erosion surface remnants have been attributed to progressive domal uplift that accompanied volcanism since middle Cenozoic time (LeMasurier & Rex 1983).

In this paper, we present new data and interpretations on the timing and style of volcanism and on the amount of relief on the unconformity at Mount Petras that differ from previous interpretations and have significant implications for reconstructions of volcanism, glacial history, and surface topography. Our analysis favours subaerial tuff cone eruptions in a shallow ice-contact environment rather than deep subglacial eruptions. We infer that there is a suggestion of, but no definitive terrestrial evidence for, Oligocene glaciation in Marie Byrd Land. Finally, we suggest that the erosional

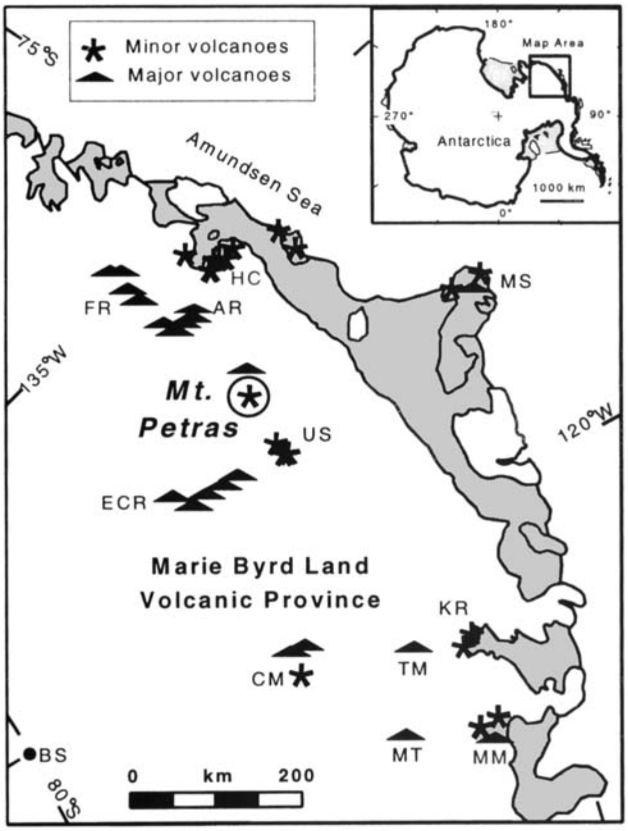


**Fig. 1.** Map of Marie Byrd Land volcanic province, located in coastal West Antarctica. Base map is from Drewry (1983) with inset map of Antarctica continent. Major volcanoes (triangles) include stratovolcanoes and shield volcanoes from 2300 to 4000 m a.s.l. and minor volcanoes (stars) include mostly smaller monogenetic volcanoes (after LeMasurier 1990b). Mount Petras is designated by an encircled star. Abbreviations: AR = Ames Range, BS = Byrd station, CM = Crary Mountains, ECR = Executive Committee Range, FR = Flood Range, HC = Hobbs Coast nunataks, KR = Kohler Range, MM = Mount Murphy, MS = Mount Siple, MT = Mount Takahe, TM = Toney Mountains, US = USAS Escarpment.

unconformity at Mount Petras exhibits relatively high topographic relief (> 400 m) that is inconsistent with a model of a single, regional, early Cenozoic low-relief unconformity in Marie Byrd Land.

## Geologic setting

Relationships between volcanism, intracontinental rifting, and final break-up of Gondwana in West Antarctica and the Ross Sea region are not well understood. An important stage in the break-up of Gondwana occurred when New Zealand and the Campbell Plateau separated from West Antarctica prior to 84 Ma (Chron 34, Lawver *et al.* 1991). Intracontinental rifting is well documented in the Ross Sea region, where the prominent rift-shoulder of the Transantarctic Mountains steps down to the Ross Sea Basin (Cooper & Davey 1985, Cooper *et al.* 1987, 1991, Fitzgerald 1992). The Ross Sea Basin consists of a series of sediment-filled horst and graben structures attributed to two rifting episodes: early rifting in the Late Cretaceous and late rifting beginning in the Eocene but intensifying in the Late Cenozoic (Cooper & Davey 1985, Cooper *et al.* 1987, 1991). The intracontinental rift zone is inferred to extend from the Ross Sea to beneath the West Antarctic ice sheet (Behrendt *et al.* 1991, 1996). On the north flank of the rift zone in West Antarctica, alkaline volcanoes of the Marie Byrd Land volcanic province have K/Ar ages as old as *c.* 25 Ma (LeMasurier 1990a). Alkaline volcanoes on both the south and north flanks of the rift are still active today (Kyle 1990, LeMasurier 1990b). The geochemistry of the West Antarctic volcanic rocks suggests a mantle plume source (Kyle *et al.* 1991, Behrendt *et al.* 1992, Hole & LeMasurier 1994). High elevation pre-volcanic erosion surfaces in Marie Byrd Land were interpreted as a topographic expression of this plume (LeMasurier & Landis 1996).

Global cooling and the earliest development of the Antarctic Ice Sheet in the earliest Oligocene (*c.* 33.7 Ma, time scale from Cande & Kent (1992)) are attributed to thermal isolation of the continent, strengthening of the circum-Antarctic current and the related major reorganization of ocean circulation patterns (Shackleton & Kennett 1975, Kennett & Barker 1990). Early Oligocene glacial diamictites, deposited on continental shelves during ice sheet expansion, were recovered from drill holes in the Ross Sea and Prydz Bay (Barrett *et al.* 1987, Hambrey *et al.* 1991). On the basis of marine data, Kennett & Barker (1990) postulated that the West Antarctic ice sheet was fully developed by the Late Miocene (*c.* 8 Ma) and achieved a stable configuration by the Early Pliocene. The pre-Late Pleistocene terrestrial record of the West Antarctic ice sheet is largely based on the volcanic record of ice magma interactions and the presence of rare interbedded tills (LeMasurier 1972a, 1972b, LeMasurier & Rex 1982, 1983, LeMasurier *et al.* 1994). LeMasurier & Rex (1982, 1983) interpreted *c.* 22–25 Ma K/Ar dated hyaloclastites at Mount Petras as the first evidence of a thick, regional ice sheet.

Mount Petras is a glacially dissected nunatak (2867 m a.s.l.), with about 900 m of relief exposed above the level of the West Antarctic ice sheet in Marie Byrd Land. LeMasurier *et al.* (1981) reported that a low-relief (< 100 m) pre-volcanic unconformity near the summit at *c.* 2700 m a.s.l. is eroded into Cretaceous rhyodacite basement rocks, K/Ar dated as 80.8 ± 5.7 Ma (LeMasurier & Wade 1976). Brief reconnaissance field work at the largest volcanic outcrop at Mount Petras, located on the south-west flank, was the basis for interpretations of the volcanic rocks as 200 m of subhorizontally stratified basaltic hyaloclastite, composed of weakly vesicular clasts, and lacking any significant subaerial component (LeMasurier 1990a). These interpretations of the deposit characteristics, together with the observation of interbedded rounded basement clasts, led LeMasurier (1990a) to conclude that the volcanic rocks were the remnants of a subglacially erupted table mountain.

https://doi.org/10.1017/S0954102000000560 Published online by Cambridge University Press

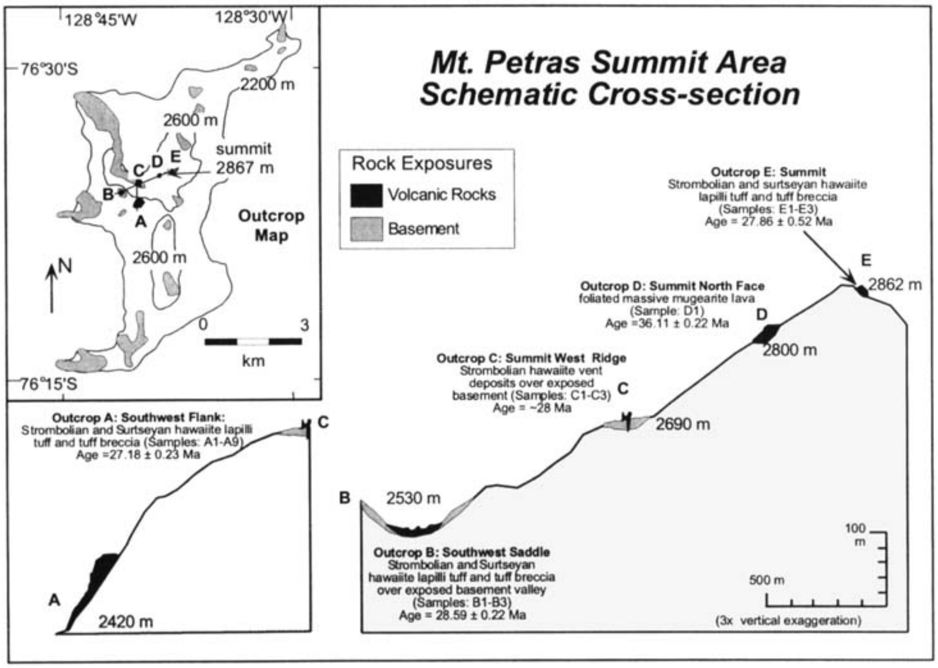


**Fig. 2.** Schematic cross-section of summit region of Mount Petras, showing the volcanic study sites. Cross-section lines A–C and B–C–D–E are shown on inset topographic map of Mount Petras outcrops. Most of Mount Petras is covered by snow and ice; basement is shown where it is exposed at the surface. Base map is from the McCuddin Mountains quadrangle, scale 1:250 000, USGS, 1973. USGS Reconnaissance Series, Antarctica, US Geological Survey.

## Methods

Fieldwork was carried out at Mount Petras in January 1994. All known outcrops were examined in detail and a total of 22 samples were collected for geochemical, petrographic and dating analysis (Fig. 2). Outcrop elevations were measured using a hand-held altimeter and elevations were corrected relative to the summit elevation of 2867 m a.s.l., as listed on the USGS topographic map.

A sedimentary facies approach was used to characterize volcanic deposits and interpret former eruptive conditions and depositional environments, following recent examples by McPhie *et al.* (1993), Smellie *et al.* (1993) and Sohn (1996). Lithofacies at Mount Petras are based on: 1) rock type (lava or clastic); 2) grain size; 3) sedimentary structures; and 4) clast characteristics (morphology, vesicularity) and componentry (after Smellie *et al.* 1993). Measurements of lithofacies features are based on visual estimates of thin sections and outcrops.

Six lava and pyroclastic bomb samples were prepared for geochemical and $^{40}Ar/^{39}Ar$ geochronological analyses. The 2–6 kg mafic rock samples were gray to black, slightly vesicular to massive, and unweathered. Major and trace element data on the six samples were obtained by standard X-ray fluorescence methods at the University of Keele (UK) on an ARL8420 spectrometer. Thin sections of lava and bomb samples were examined for mineralogy and alteration under a cross-polarizing petrographic microscope.

$^{40}Ar/^{39}Ar$ dating sample preparation and analyses were conducted at the New Mexico Geochronology Research Laboratory at the New Mexico Institute of Mining and Technology, Socorro, NM, USA. Unaltered homogeneous groundmass concentrates (200–800 μm grain size) were separated from crushed bulk samples using standard sieving, magnetic, weak HCl acid treatment, and hand-picking methods. Approximately 50 mg of each sample were placed in machined Al discs and sealed in an evacuated quartz tube along with interlaboratory neutron flux standard Fish Canyon Tuff sanidine (FCT-1 with an age of 27.84 Ma (Deino & Potts 1990) relative to a Minnesota hornblende (Mmhb-1) age of 520.4 Ma (Samson & Alexander 1987)). Samples were irradiated in the L67 position of the Ford Nuclear Reactor at the University of Michigan for 10 h (neutron flux yields approximately 0.015 J $hr^{-1}$). Following irradiation, the flux monitor crystals were placed in holes drilled in a copper planchet and fused by a $CO_2$ laser in an argon extraction system under ultra-high vacuum conditions. Neutron flux j-factors were determined from the pooled results of 4–6 single crystal analyses from six radial positions around the irradiation vessel.

The irradiated groundmass samples were incrementally-heated in 8–11 steps within a double vacuum Mo resistance furnace. Argon isotopic compositions were determined with a MAP 215–50 mass spectrometer operated in electron multiplier mode with an overall sensitivity of $2.2 \times 10^{-17}$ moles Ar/pA. The sample ages were corrected for blank, background, mass discrimination, and interfering reactions. Typical furnace blanks (including mass spectrometer backgrounds) were 24, 0.2, 0.04, 0.2, 0.1 x $10^{-16}$ moles at masses 40, 39, 38, 37 and 36 respectively. Mass discrimination measured prior to sample analyses yielded a mean value of 1.0071 ± 0.0017. The decay constant and isotopic abundances used in calculations are those suggested by Steiger & Jaeger (1977).

## Geochemistry and geochronology results

Four of the five outcrops at Mount Petras are hawaiite in composition, whereas the fifth is mugearite (Table I,

https://doi.org/10.1017/S0954102000000560 Published online by Cambridge University Press

**Table I.** X-Ray fluorescence geochemical data.

| Sample | A2 | D1 | A7 | E1 | C1 | B2 |
|---|---|---|---|---|---|---|
| F# | 323 | 332 | 329 | 333 | 337 | 343 |
| Comp. | mugearite | mugearite | hawaiite | hawaiite | hawaiite | hawaiite |
| $SiO_2$ | 50.84 | 51.24 | 47.02 | 47.30 | 47.23 | 45.87 |
| $TiO_2$ | 1.90 | 1.94 | 2.61 | 2.68 | 3.11 | 2.64 |
| $Al_2O_3$ | 14.59 | 14.33 | 16.09 | 16.21 | 14.84 | 15.73 |
| $Fe_2O_3$ | 15.47 | 15.60 | 12.62 | 12.92 | 15.88 | 13.00 |
| MnO | 0.22 | 0.23 | 0.21 | 0.21 | 0.20 | 0.21 |
| MgO | 2.20 | 2.13 | 5.78 | 6.02 | 4.15 | 6.11 |
| CaO | 6.07 | 5.54 | 8.42 | 8.38 | 6.93 | 8.46 |
| $Na_2O$ | 4.83 | 4.55 | 4.35 | 4.46 | 3.54 | 4.33 |
| $K_2O$ | 2.18 | 2.21 | 1.71 | 1.83 | 1.63 | 1.58 |
| $P_2O_5$ | 1.32 | 1.31 | 0.80 | 0.80 | 1.07 | 0.78 |
| LOI | 0.03 | 0.49 | 0.27 | 0.00 | 1.03 | 1.09 |
| **Total** | 99.65 | 99.57 | 99.89 | 100.56 | 99.62 | 99.80 |
| Ba | 814 | 882 | 521 | 487 | 485 | 510 |
| Ce | 148 | 162 | 122 | 130 | 116 | 122 |
| Cl | 159 | 60 | 214 | 268 | 158 | 241 |
| Cr | | | 137 | 133 | | 143 |
| Cu | 29 | 26 | 45 | 46 | 31 | 44 |
| Ga | 27 | 29 | 22 | 20 | 26 | 19 |
| La | 67 | 64 | 64 | 64 | 60 | 73 |
| Nb | 65 | 62 | 86 | 87 | 57 | 85 |
| Nd | 64 | 73 | 47 | 51 | 64 | 51 |
| Ni | 9 | 8 | 69 | 69 | 9 | 77 |
| Pb | 13 | 13 | 11 | 13 | 9 | 12 |
| Rb | 41 | 45 | 40 | 53 | 53 | 27 |
| S | 128 | 51 | 98 | 335 | 647 | 275 |
| Sr | 426 | 414 | 809 | 783 | 604 | 788 |
| Th | 10 | 10 | 10 | 10 | 9 | 10 |
| V | 22 | 17 | 159 | 155 | 193 | 162 |
| Y | 67 | 69 | 37 | 37 | 54 | 37 |
| Zn | 169 | 169 | 104 | 108 | 188 | 108 |
| Zr | 474 | 461 | 380 | 382 | 372 | 380 |

I.D. number designates to outcrop and sample number. F# is field sample number. Rock type classification from LeBas *et al.* (1986).

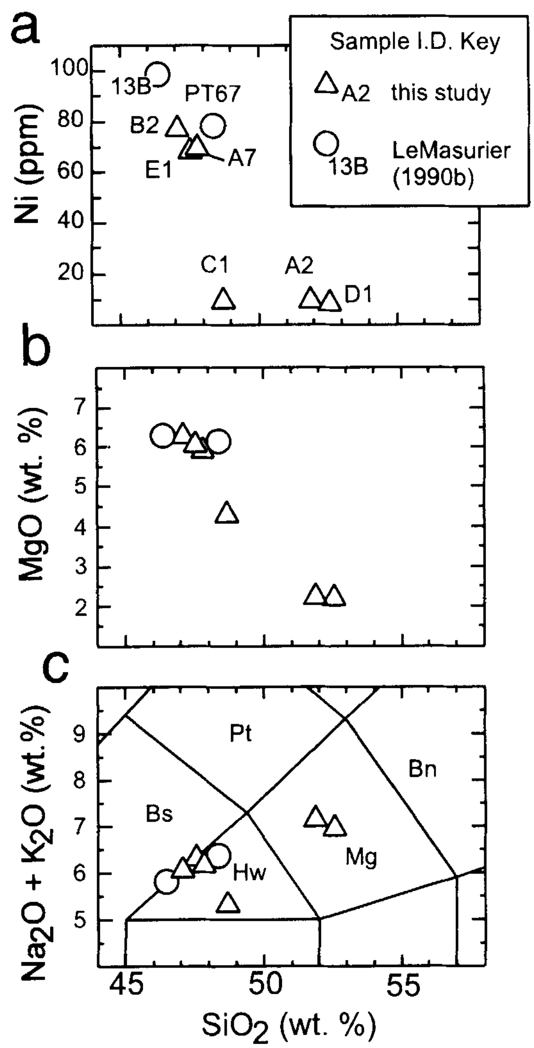


**Fig. 3 a–c.** Geochemical plots of selected major and trace elements vs silica, $SiO_2$, based on XRF analyses. All major element oxides are in weight percent, normalized to 100% water-free. Classification boundaries in 3c are after LeBas *et al.* 1986. Abbreviations: Bn = benmoreite, Bs = basanite, Hw = hawaiite, Mg = mugearite, Pt = phonotephrite. See Fig. 2 for sample outcrop locations. Sample A2 is a dense mugearite xenolith clast in hawaiite lapilli tuff.

Figs 2 & 3). The hawaiite samples are blocks and bombs from volcaniclastic rock sequences and cluster into two populations in terms of major and trace element data (Fig. 3, Table I). One hawaiite population (samples A7, B2 and E1) is compositionally close to the hawaiite/basanite boundary and is slightly more sodic and less evolved than the second hawaiite population (sample C1). Previously reported geochemical data (LeMasurier 1990a) are most similar to the less evolved hawaiite population (Fig. 3). In addition to the hawaiites, mugearite lava (sample D1) crops out just north of the summit and a chemically identical mugearite xenolith clast (sample A2) was sampled in the hawaiite volcaniclastic deposits. The mugearite lava is more evolved chemically (Fig. 3) than the hawaiites. The three distinct chemical populations possibly indicate at least three separate eruptions.

The $^{40}Ar/^{39}Ar$ age data are summarized in Table II and shown in age spectra in Fig. 4 (complete data tables are available from the authors). The samples were highly radiogenic (70–97% radiogenic $^{40}Ar$), with fairly uniform K/Ca distributions. Only one sample met the plateau criteria of Fleck *et al.* (1977); three other samples contained one step that lies slightly outside the 95% confidence interval. Four of the six Mount Petras sample ages are considered reliable; the age spectrum and isotope correlation ages of each of these samples agree within 2 $\sigma$ (Table II, Fig. 4). Two hawaiite samples (A7 and E1, Fig. 4a & d) yielded descending age spectra, which may reflect recoil redistribution of reactor-produced $^{39}Ar$ during irradiation (Turner & Cadogen 1974). Apparent ages from the steps between 600 and 1100°C comprise more than 50% of the cumulative $^{39}Ar$ released and are nearly concordant at 2 $\sigma$. The weighted means of these ages are interpreted as the best estimates of the eruption ages of each sample. One hawaiite sample (B2, Fig. 4b) produced

https://doi.org/10.1017/S0954102000000560 Published online by Cambridge University Press

a well-defined age spectrum plateau that is *c.* 7.5 Ma younger than the total fusion age. The older incremental ages, concentrated in the higher temperature steps, are associated with an increase in percent radiogenic $^{40}Ar$ composition spectrum, suggesting contamination by an older xenocryst or xenolith, possibly partially degassed Cretaceous rhyodacite.

The mugearite lava sample (D1, Fig. 4c) also produced a descending age spectrum, possibly suggestive of $^{39}Ar$ recoil or minor contamination by an older xenocrystic material. The close agreement of the total fusion, isotope correlation, and plateau ages indicates that the recoil or contamination did not have a significant effect on the age of the sample. The isotope correlation analysis of this sample produced an anomalously high non-radiogenic $^{40}Ar/^{36}Ar$ ratio (385 ± 43 compared to modern atmospheric value of 295.5), which is attributed to imprecision arising from an experimental artefact and is interpreted as imprecise and unreliable. The anomalously high trapped $^{40}Ar/^{36}Ar$ composition does not change the isotope correlation age.

The ages cluster into two groups: *c.* 36 Ma mugearite and 29–27 Ma hawaiite (Table II). The best age for the mugearite lava is 36.11 ± 0.22 Ma (Fig. 4b); the mugearite xenolith age agrees within uncertainty but the age spectrum is more discordant. The three reliable hawaiite ages (Table II, Fig. 4a, b & d) are derived from samples that appear chemically indistinguishable on the basis of XRF major element and limited trace element data. These three ages (± 2 σ uncertainties) do not overlap and the samples are tentatively interpreted to represent three chronologically distinct eruptions. The 27.18 ± 0.23 Ma $^{40}Ar/^{39}Ar$ age of the south-west flank outcrop is concordant with the 26.0 ± 1.0 Ma conventional K/Ar age from the same outcrop but is older than two other K/Ar dates, 23.6 ± 1.0 Ma and 23 ± 1 Ma, for that locality (K/Ar ages from LeMasurier & Rex 1982, 1983; ages corrected for decay constants of Steiger & Jaeger (1979) following Dalrymple (1979)). The hawaiite glass sample (C1) has a unique geochemical signature (Table I) and produced a discordant spectrum, which may reflect recoil redistribution of $^{39}Ar$ during irradiation of the glassy sample. The total fusion age of the sample, 27.90 ± 0.38 Ma, lies within the 27–29 Ma interval of hawaiite volcanism and is considered the best age estimate for that outcrop.

The $^{40}Ar/^{39}Ar$ age data combined with XRF geochemical data suggest a total of five eruptions: mugearite lava extrusion at 36 Ma and four volcaniclastic eruptions between 29 and 27 Ma. Our interpretations of $^{40}Ar/^{39}Ar$ age data indicate that Mount Petras volcanism occurred in the latest Eocene (36 Ma) and middle Oligocene (29–27 Ma) times, making it the oldest known Cenozoic alkaline volcanism in Marie Byrd Land.

## Lithofacies results

Rocks from the five Mount Petras outcrops are subdivided into two broad lithofacies categories: coherent lava, and volcaniclastic rocks (after McPhie *et al.* 1993). The coherent

**Table II.** Summary of $^{40}Ar/^{39}Ar$ age data.

| Outcrop | Sample # (F#) | Description | Total fusion data: Age ± 2σ (Ma)[1] | Total fusion data: $\%^{40}Ar_{rad}$ | Isotope correlation data: Age ± 2σ (Ma)[2] | Isotope correlation data: $^{40}Ar/^{36}Ar$ ± 2σ | Isotope correlation data: mswd | steps (°C) | $\%^{39}Ar$ | Age spectrum plateau data: Age ± 2σ (Ma)[3] | Age spectrum plateau data: $\%^{39}Ar$ | Age spectrum plateau data: $\%^{40}Ar_{rad}$ |
|---|---|---|---|---|---|---|---|---|---|---|---|---|
| A. south-west flank | A2 (323) | mugearite lava xenolith | 38.90 ± 0.30 | 93.9 | no data | | | | | **36.24 ± 0.51** | 36.0 | 96.7 |
| A. south-west flank | A7 (329) | dense hawaiite bomb interior | 26.48 ± 0.27 | 77.6 | 27.19 ± 0.72 | 295.6 ± 8.6 | 8.26 | 600–1200 | 63.2 | **27.18 ± 0.23*** | 63.2 | 87.2 |
| B. south-west saddle | B2 (343) | aphyric hawaiite lava, 2 m thick | 35.14 ± 0.38 | 72.4 | 28.56 ± 0.74 | 296.6 ± 3.0 | 3.11 | 650–950 | 52.5 | **28.59 ± 0.22** | 52.5 | 68.0 |
| C. summit west ridge | C1 (337) | aphyric glassy hawaiite lava, rare xenoliths | 27.90 ± 0.38 | 76.5 | no data | | | | | highly discordant | | |
| D. summit north face | D1 (332) | massive mugearite lava | 36.65 ± 0.21 | 97.4 | 36.03 ± 0.86 | 385 ± 43 | 1.28 | 950–1200 | 66.2 | **36.11 ± 0.22*** | 57.4 | 99.3 |
| E. summit | E1 (333) | dense hawaiite bomb interior | 27.42 ± 0.25 | 72.1 | 27.47 ± 0.69 | 315.9 ± 7.4 | 53.7 | 650–1100 | 69.3 | **27.86 ± 0.52*** | 69.3 | 81.0 |

Reliable sample age estimates in bold. F# is field sample number. [1]Total fusion age and uncertainty are weighted by $\%^{39}Ar$ in each step. $\%^{40}Ar_{rad}$ is the percent radiogenic argon in all heating steps or selected plateau steps. [2]Isochron age does not assume atmospheric value for $^{40}Ar/^{36}Ar$. [3]Plateau age and uncertainty are weighted by inverse of variance of selected, contiguous incremental ages. *Sample did not meet plateau criteria of Fleck *et al.* (1977), because one step lies slightly outside the 95% confidence interval. mswd is mean standard weighted deviation, calculation follows York (1969). Analytical tables available from T.I. Wilch.

https://doi.org/10.1017/S0954102000000560 Published online by Cambridge University Press

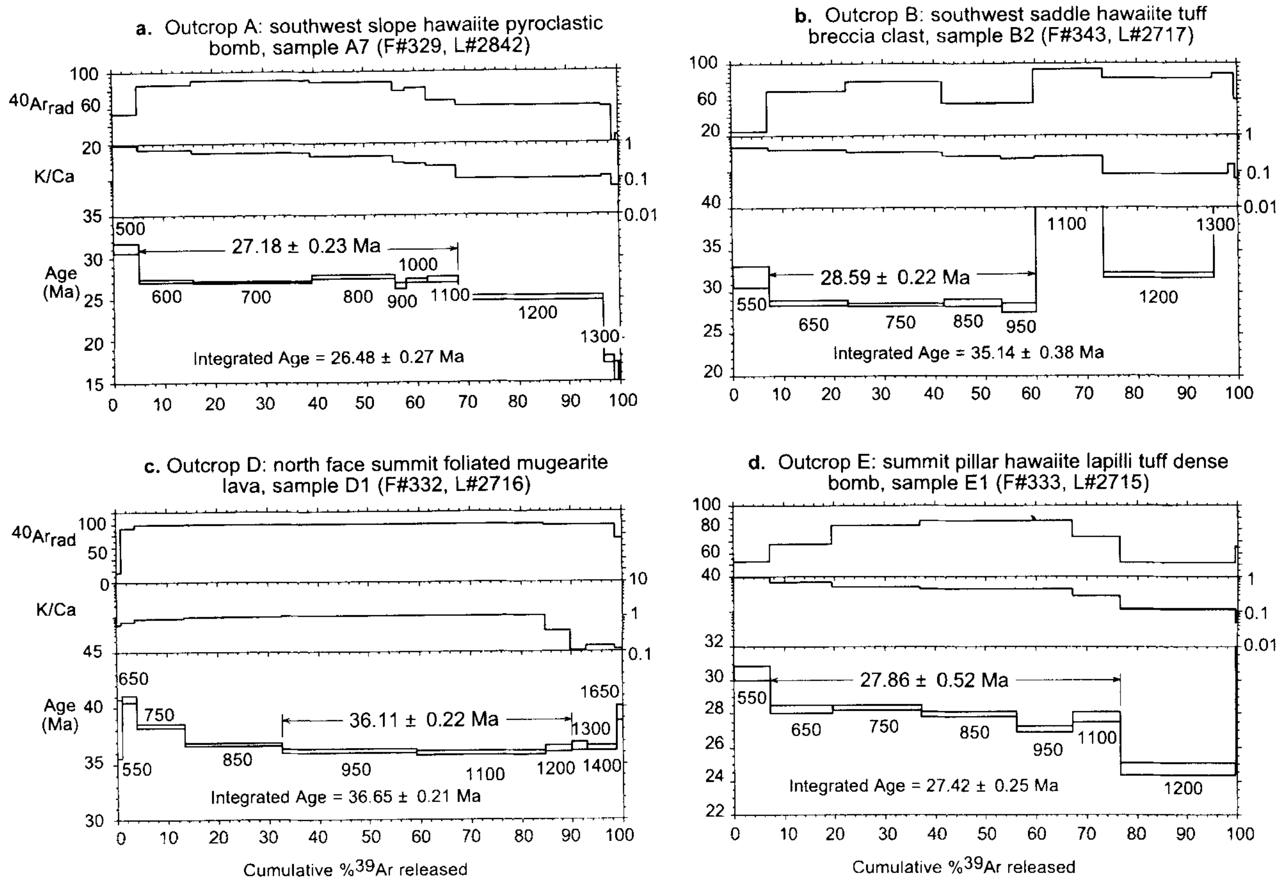


**Fig. 4 a–d.** $^{40}Ar/^{39}Ar$ age spectra of groundmass samples from four Mount Petras outcrops. Plots show percentage of cumulative $^{39}Ar$ vs apparent age, K/Ca, and % radiogenic $^{40}Ar$. Each box represents a heating step at the listed furnace temperatures (°C). The height of each box shows $\pm 2\ \sigma$ analytical uncertainty on the apparent age and $\pm 1\ \sigma$ uncertainty on the K/Ca and % radiogenic $^{40}Ar$. The width of each box designates the relative proportion of K-derived $^{39}Ar$ in each step. Variations in K/Ca are expected in multiple phase groundmass samples and reflect changes in gas composition as different minerals degas during each heating experiment.

lava consists of one outcrop of massive mugearite lava (lithofacies Lm); the volcaniclastic rocks consist of four outcrops (14 samples) of hawaiite (Fig. 2). The volcaniclastic lithofacies are given pyroclastic rock facies names, because they are composed largely of vesiculated juvenile clasts, formed by explosive fragmentation processes and there is no evidence for deposition and reworking by sedimentary processes. Two end-member lithofacies types characterize most of the pyroclastic deposits: welded tuff breccia (lithofacies TBw) and palagonitized lapilli tuff (lithofacies LT). These two types are closely associated in small and large outcrops.

*Massive lava: (lithofacies Lm): description and interpretation*

An aphyric, holocrystalline mugearite lava, $^{40}Ar/^{39}Ar$-dated to 36.11 ± 0.11 Ma, crops out on the slope just north between 2797 and 2822 m a.s.l. This lava exhibits horizontal flow-banding throughout the 25 m-thick outcrop exposure; the flow base is not exposed. We interpret this outcrop as the dense interior of a lava flow. The original volume of this lava is unknown, but the presence of 36 Ma mugearite xenoliths in the 29–27 Ma hawaiite volcaniclastic deposits more than one kilometre from *in situ* mugearite lava suggests that it was more extensive than the small outcrop that is currently exposed.

*Welded tuff breccia (lithofacies TBw): description and interpretation*

The TBw lithofacies consists of crudely stratified, steeply dipping (> 50°), incipiently to densely welded tuff breccias, composed of large, vesicular glassy bombs (up to 1 m in length) in a yellow cindery tuff breccia matrix (Fig. 5a & b). The bombs are fusiform and some have distinct reddened edges. Lesser amounts of non-welded tuff breccia containing pyroclastic bombs are associated with the TBw deposits. The matrix material of the TBw deposits is moderately palagonitized, moderately to well sorted, clast-supported, highly vesicular, subangular vitriclastic lapilli tuff (Table III). Matrix grains typically have fluidal or cuspate morphologies

https://doi.org/10.1017/S0954102000000560 Published online by Cambridge University Press

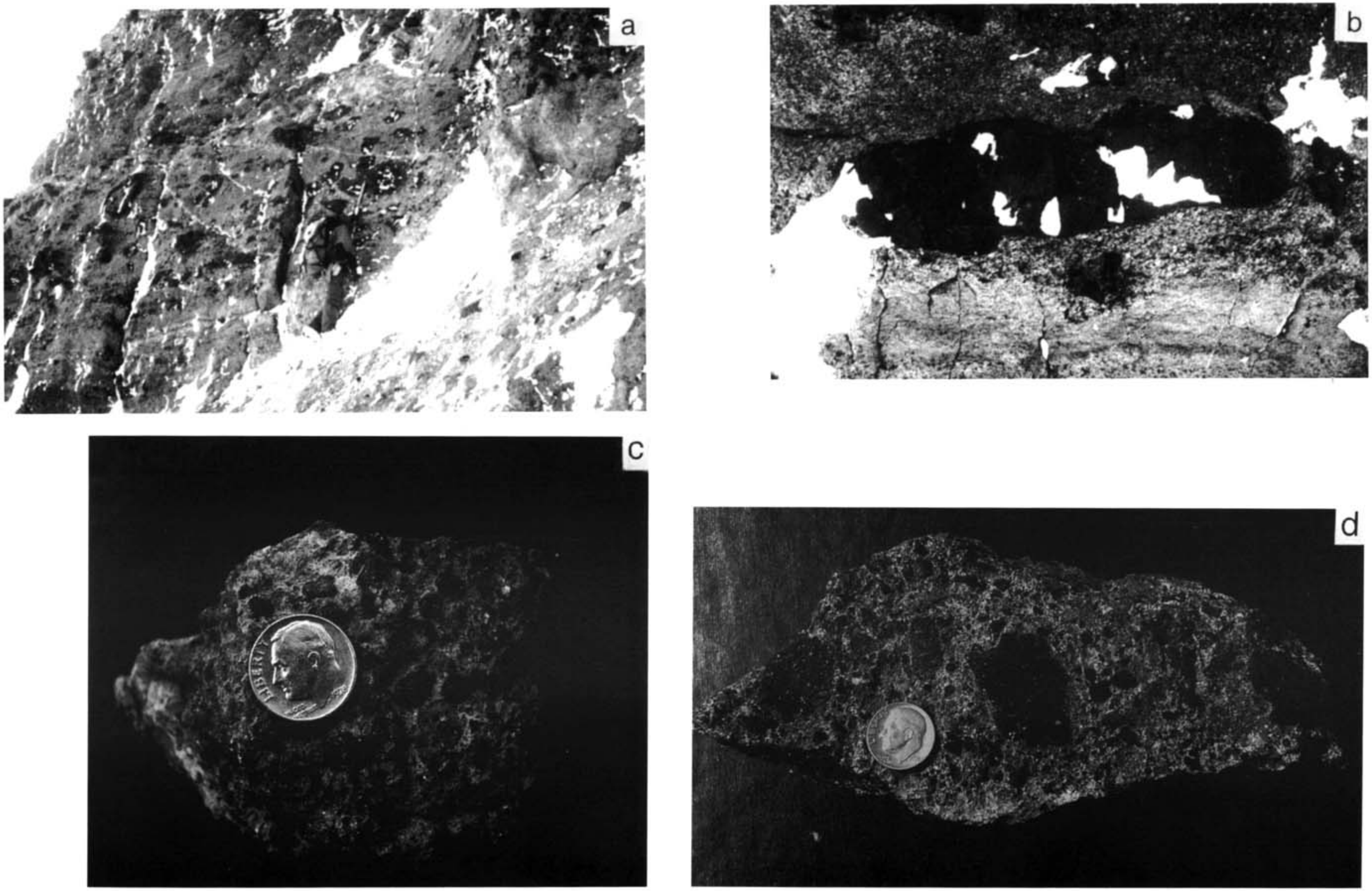


**Fig. 5. a–d.** Photographs of outcrops and hand-samples of tuff deposits. **a.** View along strike of the TBw deposit associated with outcrop A (see Fig. 2). Fusiform black volcanic bombs are exposed in a palagonitized (light coloured) lapilli tuff matrix. Person is 160 cm tall. **b.** Close-up view of an inflated but flattened volcanic bomb in a stratified lapilli tuff (LTs) matrix. Bomb is 25 cm long. Photo was taken in the upper section of outcrop A (see Figs 2 & 7). **c.** Sample of cinder-rich lapilli tuff from unit A1 (322) as described in text and shown in Table III. The clasts are variably altered glassy lapilli. Coin is 1.8 cm in diameter. **d.** Sample B1 (341) of lapilli tuff from outcrop B as shown in Table III and Fig. 2. The blocky clasts include glassy lapilli and holocrystalline hawaiite lava fragments. Coin is 1.8 cm in diameter.

and show signs of welding such as flattening of vesicles and sintered margins (Fig. 6). Rare xenolith clasts are typically glass-coated. At one locality, a densely welded breccia shows sign of post-depositional flowage in a down-dip direction. The TBw beds at the base of the upper section are continuous across the entire outcrop and thicken slightly along strike. The continuity of TBw beds is attributed to the welding at time of emplacement.

The TBw deposits are interpreted as primary ballistic fall deposits that resulted from dry, magmatic, Strombolian type eruptive phases. The depositional environment is interpreted to be subaerial to shallow subaqueous on the basis of red, deuteric oxidation of some bomb surfaces (Walker & Croasdale 1972) and welding. The welding and large sizes of bombs suggest that these are near-vent deposits. Wide ranges in vesicularity and shape of vitric clasts are common in Strombolian deposits and can result from pyroclast or cognate wall rock recycling or lava stagnation in a vent pond during an eruption (Houghton & Hackett 1984). The relative scarcity of the TBw lithofacies compared to LT lithofacies (described below) is also consistent with intermittent, mildly explosive Strombolian style eruptions.

*Lapilli Tuff (lithofacies LTs, LTm, LTa): description and interpretation*

The LT lithofacies dominates the volcaniclastic rock outcrops at Mount Petras and is subdivided into three types: stratified lapilli tuff (LTs), massive lapilli tuff (LTm), and armoured lapilli tuff (LTa) (facies codes after Sohn 1996). All LT deposits include palagonitized and fresh sideromelane glass, tachylite glass, holocrystalline hawaiite lava, plagioclase and

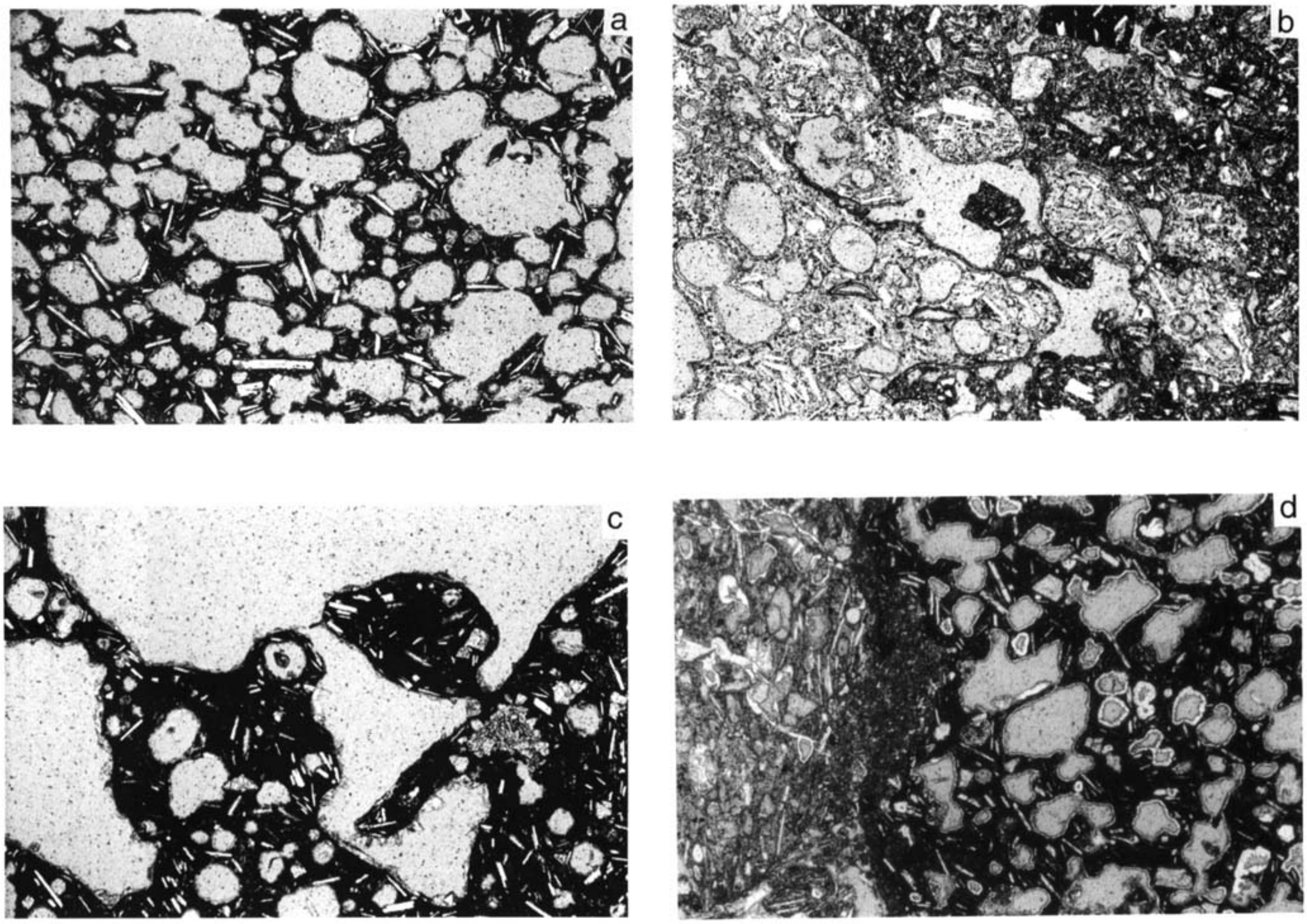


**Fig. 6. a–d.** Photomicrographs of Mount Petras hawaiite samples; thin section area covered in each photograph is 2.8 x 2.0 mm. **a.** Highly vesicular tachylite glass pyroclast from summit outcrop, sample E3. Vesicles show signs of partial coalescence. Contact between sideromelane and tachylite pyroclasts appears moulded and interlocking. **b.** Margin of fragile fluidal tachylite pyroclast from south-west flank outcrop, sample A3. Vesicularity is moderate to weak. **c.** Fluidal, moderately to highly vesicular sideromelane pyroclast (light coloured on left) and tachylite pyroclasts from summit outcrop, sample E2. **d.** Vesicular tachylite pyroclast coated by layer of fine ash, with thickness up to 350 μm, lithofacies LTa. Adjacent grain is a vesicular sideromelane pyroclast.

**Table III.** Volcaniclastic rock petrographic data.

| Sample I.D. (F#) | Deposit characterisics: grain size | bedding | sorting | grain support | clast morphology | Components: sideromelane (palagonite) % | sideromelane vesic range% | tachylite % | tachylite vesic range% | holocry. hawaiite % | lithic, crystal, other % (type) | Lithofacies sample (deposit) |
|---|---|---|---|---|---|---|---|---|---|---|---|---|
| *Outcrop A: south-west flank* | | | | | | | | | | | | |
| A1 (322) | muddy sandy gravel | planar contorted | mod | clast | cuspate, fluidal, armoured lap | 60 | 30–80 | 40 | 0–80 | | | LTs, LTa |
| A3 (325) | sandy gravel | crude planar | mod | clast | fluidal, cuspate | 45 | 30–80 | 45 | 0–80 | 10 | | LTs (TBw) |
| A4 (326) | gravel | planar | mod | clast | fluidal, blocky | 60 | 0–90 | 35 | 5–30 | 5 | tr | LTs |
| A5 (327) | sand and gravel | crude planar | mod | clast | fluidal, armoured lap | 70 | 0–85 | 30 | 0–85 | | tr | LTs, LTa |
| A6 (328) | sandy gravel | planar | poor | clast | fluidal, cuspate armoured lap | 80 | 10–75 | 15 | 0–80 | | 5 (bsmt) | LTs, LTa |
| A8 (330) | sand | planar, lensoid | well | clast | blocky, cuspate | 55 | 0–20 | 10 | 0–30 | 30 | 5 (crystal) | Ts |
| A9 (331) | muddy sandy gravel | planar | mod | clast | fluidal, blocky | 60 | 30–80 | 20 | 0–50 | 20 | | LTs |
| *Outcrop B: south-west saddle* | | | | | | | | | | | | |
| B1 (341) | sandy gravel | contorted | mod | clast | blocky | 30 | 0–50 | 15 | 0–30 | 55 | tr | LTs. |
| B3 (344) | sandy gravel | massive | mod | clast | fluidal, cuspate, blocky | 0 | | 90 | 0–90 | 10 | tr | LTm |
| *Outcrop C. summit west ridge* | | | | | | | | | | | | |
| C1 (337) | gravel | crude planar | well | clast | welded, fluidal, cuspate | 70 | 25–70 | 30 | 25–70 | | tr | L (TBw) |
| C2 (338) | muddy sandy gravel | crude planar | mod | clast | fluidal, cuspate | 60 | 15–70 | 20 | 15–70 | 15 | 5 (bsmt) | LTs (TBw) |
| C3 (339) | muddy sandy gravel | massive | poor | clast | blocky, fluidal | 60 | 0–75 | 15 | 10–65 | 5 | 20 (f.g., juv, bsmt) | LTm |
| *Outcrop E: summit* | | | | | | | | | | | | |
| E2 (335) | muddy gravel | planar | poor | matrix | fluidal, blocky, armoured lap | 60 | 40–80 | 5 | 50–70 | 20 | 15 (f.g., juv) | LTs, LTa |
| E3 (336) | muddy sandy gravel | planar | mod | mixed | fluidal, blocky | 20 | 0–75 | 20 | 10–90 | 40 | 20 (f.g., juv) | LTs |

Notes: Outcrop localities (italics) are shown in Fig. 2. F# is field sample number. Bedding from field observations. Component analysis based on visual estimates of thin-sections.

Abbreviations: mod = moderate, tr = trace, bsmt = basement, f.g. = fine-grained, juv = juvenile. Facies code abbreviations: LT = lapilli tuff, L = lapillistone, TB = tuff breccia, s = stratified, a = armoured, w = welded, m = massive.

https://doi.org/10.1017/S0954102000000560 Published online by Cambridge University Press

olivine crystal fragments, mugearite xenoliths, and rhyodacite xenoliths (Table III). Sideromelane and tachylite glass clasts typically comprise more than 75% of deposits, contain fine-grained microphenocrysts (< 500 mm) of plagioclase, olivine and clinopyroxene and exhibit a wide range of vesicularity from 0–90% (Figs 5c & 6). Among the clast types are fluidal and cuspate glass shards and blocky glass and lithic fragments (Fig. 5c & d). Fluidal grains have smooth, rounded or spiny margins, are highly vesiculated (> 50%), and commonly broken (Fig. 6c). Cuspate shards have angular intersecting concave grain boundaries formed by fragmentation of thin vesicle walls. Blocky grains are subangular to subrounded and are poorly vesiculated (0–30%). A thin veneer of very fine ash particles (typically 100 mm thick) coats some but not all blocky coarse ash and fine lapilli grains in armoured lapilli tuff units (LTa). These ash coatings have non-uniform thicknesses (50–350 mm) and appear to consist of fine-grained (*c.* 5 mm diameter) glass and crystal fragments (Fig. 6d). Some lithic grains are coated by a layer of coherent glass.

Both the LTm and LTs lithofacies contain rare (0–5%) large lithic clasts and pyroclasts. The lithic clasts are subangular to subrounded basement and mugearite blocks, which are up to 10 cm in diameter and sometimes coated with hawaiite lava. No signs of glacial moulding or polish were observed on any of the lithic clasts. Intact and broken pyroclastic bombs and blocks occur as large clasts up to 30 cm in length in some deposits.

The LT facies are moderately sorted, clast-supported, and either massive (LTm) or planar bedded (LTs and LTa). Bed thickness ranges from 1–20 cm. Bedding planes typically dip steeply (20–90°). The beds can be traced continuously across smaller outcrops (< 15 m diameter), but are discontinuous and pinch out in larger outcrops. Contacts between the LT lithofacies and the TBw lithofacies appear conformable. At one outcrop, a lobe of coherent holocrystalline lava is brecciated laterally into massive lapilli tuff (LTm). The LT deposits are moderately palagonitized and weakly cemented by secondary smectite, calcite, and/or zeolite minerals.

Lateral lithofacies changes in the LT outcrops are difficult to observe because of the limited extent of most outcrops. In general, beds appeared to be continuous across the 5–15 m strike length of most outcrops. However, in lower sections of the south-west flank outcrop, LT beds cannot be traced laterally more than 10 m. The LT bed contacts in this section do not appear to be erosive. The lateral discontinuity of beds suggests that the clasts were remobilized by mass flow processes on the steep side-slopes, as was observed in Korean tuff cones (Sohn 1996).

Features of the LT lithofacies are consistent with both "dry" magmatic and "wet" phreatomagmatic eruptive phases. Diagnostic features of "dry" magmatic eruptions are fusiform pyroclastic bombs, lava-coated and glass-coated lithic clasts, and scoriaceous and fluidal droplet lapilli and ash grains. Similar large fusiform bombs at Ilchulbong tuff cone, South Korea were attributed to periodic, dry Strombolian eruptions in between hydromagmatic explosions (Sohn & Chough 1992). The lack of bomb and block sags may indicate slight reworking on steep slopes. The lava-coated and lava-free, subangular to subrounded lithic clasts are interpreted as xenoliths eroded and crudely milled during magmatic and phreatomagmatic eruptions, respectively. The fluidal droplet morphologies of lapilli clasts are formed by surface tension and are indicative of subaerial Strombolian eruptions (Walker & Croasdale 1972). An analogue for the inferred mixed magmatic/phreatomagmatic eruption at Mount Petras is the 1963–67 eruption of Surtsey volcano, Iceland, which was an emergent tuff cone dominated by continuous uprush and jetting of tephra, steam, and water, with intermittent Hawaiian-style activity in "dry" vent conditions (Thorarinsson *et al.* 1964). The type "Surtseyan" eruption characterizes one style of phreatomagmatic eruption, in which interactions between vesiculating magma and a water-laden tephra slurry drive the eruption (Kokelaar 1986).

Lithofacies features indicative of phreatomagmatic eruptions include: clasts that are heterogeneous in composition, morphology and vesicularity (Wohletz 1983, Kokelaar 1986, Houghton & Schmincke 1989, Houghton & Wilson 1989), well-developed but often contorted planar bedding (Wohletz 1983, Sohn 1996), and armoured lapilli beds (Waters & Fisher 1971) (Table III). Induration and palagonitization are useful indicators of phreatomagmatic eruptions for young deposits but are more equivocal indicators for old deposits (Wohletz 1983). The lithofacies characteristics are interpreted to result from a combination of magmatic explosivity and phreatomagmatic explosivity (Kokelaar 1986). The predominance of coarse-grained clasts (lapilli) in the Mount Petras deposits favours less energetic Surtseyan style eruptions rather than highly energetic "Taalian" style surges (see summary discussion in Wohletz & Heiken 1992). The low percentage of xenolith clasts (< 10%) and lava-coating of some of the clasts suggest that the fragmentation depth was relatively shallow (Sohn 1996). Some erosion and reworking of beds is inferred from discontinuous nature of beds in large outcrops. Changes in bedding and grain-size characteristics (e.g. ash-rich massive beds versus lapilli-rich planar beds) are attributed to variations in water:magma mixing ratios, and geologic and hydrologic conditions (Sohn 1996). Possible eruption recycling of clasts is suggested by uneven mud-coating on some clasts in the LTa deposits and the mixture of fluidal and blocky clasts (Houghton & Smith 1993). Other explanations for the heterogeneous assortment of poorly and highly vesiculated tachylite, sideromelane and holocrystalline clasts include hydromagmatic interactions between highly vesiculated magma and wet poorly vesiculated tephra, partially degassed magma, and/or wall-rock in the vent (Houghton & Hackett 1984, Kokelaar 1986). The absence of traction bedforms such as cross-bedding favours deposition from either wet pyroclastic fall or wet surge processes. The LT lithofacies are interpreted as products of wet Surtseyan style eruptive phases, dominated by tephra finger jets, wet surges

https://doi.org/10.1017/S0954102000000560 Published online by Cambridge University Press

and pyroclastic fall processes.

The over-steepened beds (> 45° for wet, mud-rich sediments) are attributed to post-depositional collapse phenomena at or near the crater rim of tuff cones (see discussion by Sohn 1996). This interpretation is consistent with a model by Sohn (1996) that suggests that the morphology of phreatomagmatic tuff cone volcanoes is controlled largely by the dominant pyroclastic fall deposition, followed by remobilization and deformation of deposits on steep, unstable slopes.

A subaerial or very shallow water depositional environment is inferred on the basis of interbedded, welded pyroclastic deposits (TBw) (Fig. 5a & b). A subaqueous eruption in a cupola of steam as described by Kokelaar (1986) could explain the highly vesiculated tachylite pyroclasts but not the presence of welded and deuterically oxidized beds. Lava intruded into and intermixed with tephra (LTm) at one outcrop is suggestive of magma interaction with wet tephra in a near-vent tuff cone setting (Kokelaar 1986, Sohn 1996). The limited exposures do not allow reconstruction of volcano morphology, except to state that the presence of steep-dipping lapilli tuff strata is also consistent with near-vent tuff cone facies rather than tuff ring facies (Sohn 1996).

*Pyroclastic lithofacies associations*

Stratigraphic relationships among pyroclastic lithofacies and the inferred eruption histories of the four hawaiite outcrops are summarized in Table IV and shown by example in Fig. 7. All of the pyroclastic lithofacies are interpreted as products of mildly explosive eruptions, ranging from wet, Surtseyan to dry, Strombolian in style. Figure 7 shows vertical lithofacies variations in a > 40 m thick stratigraphic section located on the south-west flank outcrop A (Fig. 2a), from which alternating eruption styles can be inferred. The stratigraphic section can be divided into two parts: the lower 15 m of the section is characterized by well bedded, finer grained lapilli tuffs with up to 10% non-juvenile lithic clasts (LTm, LTs and LTa lithofacies); and the upper 25 m of the section is characterized by coarser grained lapilli tuff (LTs) and welded to non-welded tuff breccia (TBw) with oxidized pyroclastic bombs up to 1 m in length. The relative abundance of juvenile material (i.e. intact and fragmented vitric clasts) increases up section. Overall, the pyroclastic rocks are well-bedded, with northward dipping beds that steepen to > 70° up section.

Vertical lithofacies changes are characterized by alternating Surtseyan (LTa, LTs, LTm) and Strombolian lithofacies (TBw and some LTs), indicative of fluctuations of external water during eruptions (Fig. 7). The conformable contacts throughout the outcrop suggest a single eruption or series of eruptions without significant time hiatuses (i.e. no time for erosion). In many cases, eruptive sequences progressed from wet Surtseyan to dry Strombolian conditions. All of the Mount Petras outcrops exhibit characteristics of a near-vent, subaerial tuff cone setting, including steeply dipping, contorted, and discontinuous planar beds, large pyroclastic bombs (to 1 m),

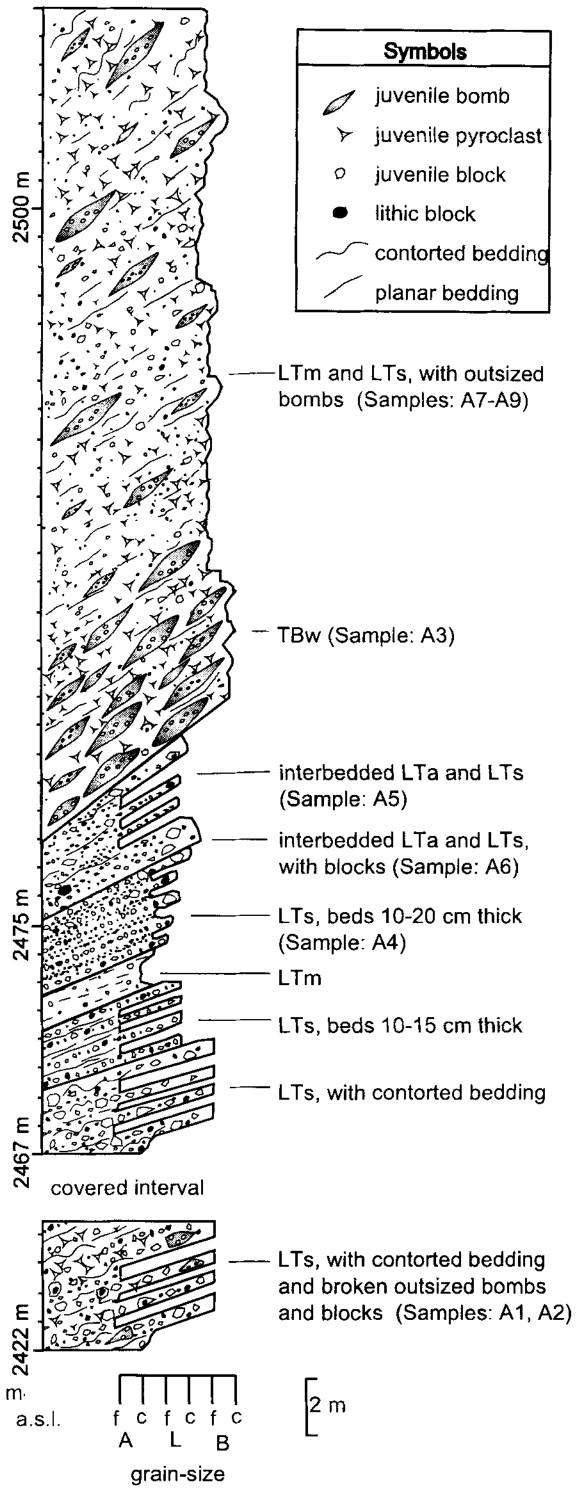


**Fig. 7.** Outcrop log of 40 m thick stratigraphic section on the south-west flank of Mount Petras (see Fig. 2, outcrop A for location). Beds dip steeply into the slope (to the north). Grain size abbreviations: A = ash, L = lapilli, B = block or bomb, c = coarse, f = fine. Lithofacies abbreviations: L = lapilli, T = tuff, B = breccia, a = armoured, m = massive, s = stratified, w = welded.

https://doi.org/10.1017/S0954102000000560 Published online by Cambridge University Press

**Table IV.** Outcrop descriptions and interpretations, locations shown in Fig. 2.

| Location | Elevation | Age ± 2σ | Lithofacies |
|---|---|---|---|
| *Outcrop A: south-west flank* | 2422–2517 m | 27.18 ± 0.23 Ma | TBw, LTs, LTa, LTm |
| Description: | Most extensive exposures at Mount Petras consist of two outcrops. The smaller outcrop is about 10 x 50 m in size and is the lowest *in situ* outcrop at Mount Petras. It consists of slightly convoluted LTs and LTm lithofacies dipping 30°N that contain numerous large juvenile pyroclastic bombs and lava-coated mugearite xenoliths. The larger outcrop is at least 100 x 100 m in area and includes a > 40 m-high stratigraphic section, Fig. 7. Stratigraphic section is described in text. | | |
| Interpretation: | Near-vent primary pyroclastic fall and reworked fall tuff cone deposits. Eruption style progressed through four stages: 1. Surtseyan with intermittent Strombolian, 2. wet Surtseyan, 3. dry Strombolian, and 4. Surtseyan with intermittent Strombolian. | | |
| *Outcrop B: south-west saddle* | 2532–2537 m | 28.59 ± 0.22 Ma | TBw, LTs, LTm |
| Description: | Isolated outcrops with no apparent stratigraphic situated in a bedrock saddle. Lithofacies include welded tuff breccia, intrusive lava brecciating into a massive lapilli tuff slurry, stratified lapilli tuff with large pyroclastic bombs. | | |
| Interpretation: | Tuff cone vent deposits with Surtseyan and Strombolian facies. | | |
| *Outcrop C: summit west ridge* | 2682–2692 m | 27.90 ± 0.38 Ma | TBw, LTm |
| Description: | A 10 x 20 m outcrop that overlies bedrock and consists of two steeply dipping units. A densely welded tuff breccia flanked by massive lapilli tuff, overlying bedrock. | | |
| Interpretation: | Tuff cone vent facies. Eruption style progressed from wet Surtseyan to dry Strombolian. | | |
| *Outcrop D: summit north face* | 2797–2822 m | 36.11 ± 0.22 Ma | Lm |
| Description: | Massive mugearite lava exposed in 25 m thick section on slope just north of summit. Lava is horizontally foliated, holocrystalline, and aphyric. | | |
| Interpretation: | Product of effusive eruption. No associated pyroclastic rocks or autoclastic breccias exposed. | | |
| *Outcrop E: summit* | 2852–2862 m | 27.86 ± 0.52 Ma | LTs |
| Description: | An approximately 10 m high outcrop, located 200 m west of the true summit, consists of near vertically oriented, interbedded fine and coarse lapilli tuff. Fluidal droplet lapilli pyroclasts common. | | |
| Interpretation: | Near-vent, tuff and cinder cone deposits. Mixed Strombolian and Surtseyan eruption. | | |

welding and deuteric oxidation, and brecciated intrusive hawaiite.

## Discussion

### *Pre-volcanic erosion surface*

Hawaiite pyroclastic rocks situated in the south-west saddle at 2690 m. a.s.l. (Fig. 2a) and the summit west ridge at 2530 m. a.s.l. (Fig. 2c) overlie bedrock, indicating a minimum of 160 m of vertical relief on the pre-hawaiite unconformity (Fig. 2). The position of 29–27 Ma *in situ* hawaiite rocks down to elevations of 2422 m a.s.l. extends the minimum vertical relief on the pre-hawaiite unconformity to 270 m. Finally, the presence of the 36 Ma mugearite lava at elevations up to 2822 m a.s.l. further extends the minimum vertical relief on the pre-hawaiite unconformity to 400 m. We observed no evidence for faulting during or since volcanism and our estimate of 400 m of relief assumes that little or no displacement has occurred. The relatively high relief on the unconformity is consistent with an environment of active erosion at the time. The interval of erosion covers 50 Ma and is bracketed by the underlying *c.* 80 Ma rhyodacite and the *c.* 29 Ma hawaiite.

The inference here of > 400 m relief on the unconformity at Mount Petras is inconsistent with a previous estimate of < 100 m based on reconnaissance observations made from a helicopter (LeMasurier 1990a). The previously reported low relief on the unconformity at Mount Petras was used to help support the hypothesis of the West Antarctic erosion surface (WAES) as a single Early Cenozoic erosion surface (LeMasurier & Landis 1996). Elsewhere in Marie Byrd Land, pre-volcanic erosion surfaces are reported as being flat (< 100 m of relief) and overlain by mostly Late Miocene and Pliocene volcanic rocks (LeMasurier & Landis 1996). We find no evidence at Mount Petras to support a model of a low-relief, early Cenozoic WAES, nor is there evidence for a postulated early Cenozoic marine planation of West Antarctica. On the contrary, exposed rocks at Mount Petras suggest an environment of active erosion at the time. The fact that the volcanic outcrops at Mount Petras are preserved as erosional remnants suggests that there has been abundant post-volcanic erosion.

### *Eruption history at Mount Petras*

Five eruptions at Mount Petras are identified on the bases of $^{40}Ar/^{39}Ar$ ages, geochemistry, lithofacies analysis, and field relations. The first stage of volcanism occurred at 36.11 ± 0.22 Ma with an apparently dry extrusion of massive mugearite lava. The second stage of eruptions includes four hawaiite pyroclastic events between 29 and 27 Ma. The first of these events were Surtseyan and Strombolian eruptions in the

https://doi.org/10.1017/S0954102000000560 Published online by Cambridge University Press

south-west saddle area at 28.59 ± 0.22 Ma. The next eruptions occurred at 27.90 ± 0.38 Ma (?) and 27.86 ± 0.52 Ma, with deposition of Surtseyan and Strombolian lapilli tuff and welded pyroclastic rocks at the summit west ridge and summit areas (outcrops C and E, respectively). The final phase of volcanism produced 27.18 ± 0.23 Ma tuff cone material on the south-west flank (outcrop A). Each of the hawaiite outcrops are interpreted as vent complexes or near-vent lithofacies that resulted from subaerial Surtseyan and Strombolian eruptions from three different vents (Fig. 2).

Our analysis does not support previous field interpretations of the volcanic rocks as subglacial hyaloclastite erosional remnants of a volcanic table mountain. Instead, lithofacies associations, ages and outcrop distributions (discussed below) suggest limited syneruptive glacial ice, and thus argue against the existence of a thick regional ice-sheet in West Antarctica during Oligocene times (LeMasurier *et al.* 1981).

### *Eruptive and depositional environment at Mount Petras*

All of the 29–27 Ma pyroclastic outcrops are derived in part from Surtseyan eruptions, which require interaction between magma and water (possibly melted ice) or wet sediments. In broad terms, there are three possible environments for water-magma interactions: subterranean (groundwater) environment; deep subaqueous (subglacial) environment, and shallow subaqueous (subglacial) to subaerial environment.

Interaction with deep-seated groundwater is ruled out because of the low number of basement clasts and the abundance of highly vesiculated pyroclasts in all of the deposits (Wohletz 1983, Leat & Thompson 1988, Houghton & Schmincke 1989, Sohn 1996). The inclusion of rare rhyodacite and mugearite lithic clasts in the pyroclastic deposits suggest limited interaction with groundwater at a shallow depth. Such limited interaction is supported by the presence of basement lithic clasts coated by juvenile glass in some deposits (Houghton & Schmincke 1989).

An alternative model for the origin of the Mount Petras outcrops is that the eruptions ejected material directly into a relatively deep subaqueous environment, with no contact with open-air. This alternative requires that the apparent subaerial eruption features formed in cupola of steam and tephra as is envisioned to have occurred at submarine volcano Surtla, Iceland (Kokelaar 1986). Grab-samples from the submarine volcanic edifice at Surtla include deuterically oxidized (reddened) and agglutinated pyroclasts and one deformed, 22 cm long spatter bomb. The cupola model for the Mount Petras rocks cannot be disproved, but it is not preferred for the following reasons: the lack of glacial, lacustrine, or marine sedimentary deposits mixed in with or underlying the volcanic outcrops, the lack of tractional sedimentary structures common in subaqueous environments, the lack of pillows in the mugearite lava deposit, and the very extensive zone of bomb welding in deposits at the south-west flank outcrop A.

We conclude that eruptions in shallow subaqueous to subaerial environments best explain our observations. Three possible types of shallow subaqueous environments are evaluated below:

1) Sea water. The suggestion by LeMasurier & Landis (1996) that the erosion surface formed by early Cenozoic marine planation would be consistent with a sea water source for phreatomagmatic interaction. Although sea water has been an important source of water in many tuff cone eruptions, it seems unlikely at Mount Petras given the lack of marine fossils or clays, lack of tractional bedforms as seen elsewhere (Thorarinsson *et al.* 1964, Kokelaar & Durant 1983, Cas *et al.* 1989), and, more important, the requirement for > 400 m of sea level variation in < 2 Ma. The total change in global sea level from the Last Glacial Maximum to an ice-free world would be only 200 m.
2) Surface water (stream or lake). Stream and lake water are considered unlikely sources of external water because of the lack of fluviatile or lacustrine sediments as lithic clasts in the volcanic deposits and as preserved deposits on the landscape. Furthermore, both lake and stream interactions would require fairly complicated palaeohydrologic settings: four perched shallow lakes at different elevations or a streams that intersect outcrop sites distributed along present ridge lines over a few kilometres.
3) Glacial meltwater. The deposits at Mount Petras are similar to the uppermost deposits of volcanic table mountain sequences, associated with eruptions that have emerged above water level in confined englacial lakes (Jones 1969, Skilling 1994). Volcanic table mountains are glacial volcanic edifices that grow in several stages: beginning with effusion of pillow lavas under high confining pressures, followed by hydromagmatic explosions of fine tuffs under low confining pressures, and culminating in mildly explosive and effusive subaerial cinder cone/lava eruptions with an associated subaqueous flow foot delta forming where lava enters englacial lake (Jones 1969). Recent models of englacial volcanism show the same basic progression of eruptive conditions and lithofacies as in the table mountain models but include reworking of deposits as an additional important process and differentiate eruptions in thick-ice/ponded-water environments from those in thin-ice/flowing-water environments (Skilling 1994, Smellie & Skilling 1994, Smellie & Hole 1997). Mount Petras outcrops differ from table mountain and other englacial volcanic sequences in that they show no signs of deep-water:magma interactions, such as poorly vesiculated pillow lavas and hyaloclastite breccias. Only vesiculated Surtseyan and Strombolian tuffs occur where volcanic rocks are exposed in contact with basement rocks. The Surtseyan style eruptions at Mount Petras are consistent with eruptions through shallow water or wet tephra

Subaqueous to emergent eruption of highly vesiculated magma through shallow englacial lakes, possibly associated with a small ice cap or a veneer of slope ice, is consistent with many features of the Mount Petras outcrops including: the heterogeneous juvenile clast populations, the lack of fossil-bearing sediments, the lack of wave re-working, the outcrop elevation variations, the geographic distribution of the outcrops, and the possibility of fluctuating water-levels during individual eruptions. When volcanoes erupt through a glacier or ice sheet, two common components are glacial unconformities and glacially striated or moulded clasts. However, at Mount Petras, there is no evidence for pre-volcanic glacial deposits. *Our preferred explanation* for the Mount Petras outcrops is that they result from hydromagmatic interactions fed by melting of a thin veneer of ice. A thin-ice environment is consistent with the lack of glacial deposits and with the apparently random distribution of the volcanic centres on the landscape. The fluctuations between dry and wet eruptive conditions can be explained by meltwater draining and refilling shallow englacial ice chambers.

## Summary

The volcanic history of Mount Petras provides new data for interpretations of mid-Cenozoic volcanism, glaciation, and landscape evolution in Marie Byrd Land, West Antarctica. Five eruptions are inferred from $^{40}Ar/^{39}Ar$ dating, XRF geochemistry and field analyses. Onset of Cenozoic alkaline volcanism in Marie Byrd Land occurred at 36.11 ± 0.11 Ma, with the eruption of massive mugearite lava near the summit of Mount Petras. Four pyroclastic eruptions of mixed Surtseyan and Strombolian style produced hawaiite composition rocks between *c.* 29 and 27 Ma. These subaerial eruptions involved intermittent interaction with water derived from a thin, local ice cap or snow and ice on the slopes of a relatively high relief (> 400 m) bedrock nunatak. The *c.* 29–27 Ma pyroclastic deposits at Mount Petras provide the oldest terrestrial evidence for glacial ice in Marie Byrd Land but offer no evidence for a thick, continental ice sheet at that time.

## Acknowledgements

This work was supported by the National Science Foundation (NSF-DPP918806), with additional funding from the New Mexico Geochronological Research Laboratory. We thank US Navy VXE-6 squadron, Antarctic Support Associates, and Ken Borek Air Ltd for logistical support; Nelia Dunbar and Tony Teeling for field assistance; John Smellie, British Antarctic Survey, for providing XRF data from the University of Keele, and Nelia Dunbar, Philip Kyle, Kurt Panter, and Gary Smith for useful criticism of the manuscript.

## References

Barrett, P.J., Elston, D.P., Harwood, D.M., McKelvey, B.C. & Webb, P.N. 1987. Mid-Cenozoic record of glaciation and sea-level change on the margin of the Victoria Land basin, Antarctica. *Geology*, **15**, 634–637.

Behrendt, J.C., LeMasurier, W. & Cooper, A.W. 1992. The West Antarctic rift system - a propagating rift "captured" by a mantle plume? *In* Yoshida, Y., Kaminuma, K. & Shiraishi, K., *eds. Recent progress in Antarctic earth science*. Tokyo: Terra Scientific Publishing Company, 315–322.

Behrendt, J.C., LeMasurier, W.E., Cooper, A.K., Tessensohn, F., Trehu, A. & Damaske, D. 1991. Geophysical studies of the West Antarctic rift system. *Tectonics*, **10**, 1257–1273.

Behrendt, J.C., Saltus, R., Damaske, D., McCafferty, A., Finn, C.A., Blankenship, D.D. & Bell, R.E. 1996. Patterns of late Cenozoic volcanic and tectonic activity in the West Antarctic rift system revealed by aeromagnetic data. *Tectonics*, **15**, 660–676.

Cande, S.C. & Kent, D.V. 1992. A new geomagnetic polarity time scale for the Late Cretaceous and Cenozoic. *Journal of Geophysical Research*, **97**, 13 917–13 952.

Cas, R.A.F., Landis, C.A. & Fordyce, R.E. 1989. A monogenetic, Surtla-type, Surtseyan volcano from the Eocene–Oligocene Waiareka–Deborah volcanics, Otago, New Zealand: a model. *Bulletin of Volcanology*, **51**, 281–298.

Cooper, A.K. & Davey, F.J. 1985. Episodic rifting of Phanerozoic rocks in the Victoria Land basin, Western Ross Sea, Antarctica. *Science*, **229**, 1085–1087.

Cooper, A.K., Davey, F.J. & Behrendt, J.C. 1987. Seismic stratigraphy and structure of the Victoria Land basin, western Ross Sea, Antarctica. *In* Cooper, A.K. & Davey, F.J., *eds. The Antarctic Continental Margin: geology and geophysics of the Western Ross Sea*. Houston, TX: Circum-Pacific Council for Energy and Mineral Resources, 27–65.

Cooper, A.K., Davey, F.J. & Hinz, K. 1991. Crustal extension and origin of sedimentary basins beneath the Ross Sea and Ross Ice Shelf, Antarctica. *In* Thomson, M.R.A., Crame, J.A. & Thomson, J.W., *eds. Geological evolution of Antarctica*. Cambridge: Cambridge University Press, 299–304.

Dalrymple, G.B. 1979. Critical tables for conversion of K/Ar ages from old to new decay constants. *Geology*, **7**, 558–560.

Deino, A. & Potts, R. 1990. Single-crystal $^{40}Ar/^{39}Ar$ dating of the Olorgesailie Formation, Southern Kenya Rift. *Journal of Geophysical Research*, **95**, 8453–8470.

Drewry, D.J. 1983. *Antarctica: glaciological and geophysical folio*. Cambridge: Scott Polar Research Institute.

Fitzgerald, P.G. 1992. The Transantarctic Mountains of southern Victoria Land: the application of apatite fission track analysis to a rift shoulder uplift. *Tectonics*, **11**, 634–662.

Fleck, R.J., Sutter, J.F. & Elliot, D.H. 1977. Interpretation of discordant $^{40}Ar/^{39}Ar$ age spectra of Mesozoic tholeiites from Antarctica. *Geochimica et Cosmochimica Acta*, **41**, 15–32.

Hambrey, M.J., Larsen, B. & Ehrmann, W.U. 1991. The glacial record from the Prydz Bay continental shelf, East Antarctica. *Proceedings of Ocean Drilling Program Scientific Results*, **119**, 77–132.

Hole, M.J. & LeMasurier, W.E. 1994. Tectonic controls on the geochemical composition of Cenozoic mafic alkaline volcanic rocks from West Antarctica. *Contributions to Mineralogy and Petrology*, **117**, 187–202.

Houghton, B.F. & Hackett, W.R. 1984. Strombolian and phreatomagmatic deposits of Ohakune craters, Ruapehu, New Zealand: a complex interaction between external water and rising basaltic magma. *Journal of Volcanology and Geothermal Research*, **21**, 207–231.

Houghton, B.F. & Schmincke, H.U. 1989. Rothenberg scoria cone, East Eifel: a complex Strombolian and phreatomagmatic volcano. *Bulletin of Volcanology*, **51**, 28–48.

Houghton, B.F. & Smith, R.T. 1993. Recycling of magmatic clasts during explosive eruptions: estimating the true juvenile content of phreatomagmatic volcanic deposits. *Bulletin of Volcanology*, **55**, 414–420.

Houghton, B.F. & Wilson, C.J.N. 1989. A vesicularity index for pyroclastic deposits. *Bulletin of Volcanology*, **51**, 451–462.

Jones, J.G. 1969. Intraglacial volcanoes of the Laugarvatn region, south-west Iceland. *Journal of the Geological Society, London*, **124**, 197–211.

Kennett, J.P. & Barker, P.F. 1990. Latest Cretaceous to Cenozoic climate and oceanographic developments in the Weddell Sea, Antarctica: an ocean-drilling perspective. *Proceedings of the Ocean Drilling Program, Scientific Results*, **113**, 937–958.

Kokelaar, B.P. & Durant, G.P. 1983. The submarine eruption and erosion of Surtla (Surtsey), Iceland. *Journal of Volcanology and Geothermal Research*, **19**, 239–246.

Kokelaar, B.P. 1986. Magma-water interactions in subaqueous and emergent basaltic volcanism. *Bulletin of Volcanology*, **48**, 275–289.

Kyle, P.R. 1990. McMurdo Volcanic Group - western Ross Embayment. *Antarctic Research Series*, **48**, 19–25.

Kyle, P.R., McIntosh, W.C., Panter, K.S. & Smellie, J.L. 1991. Is volcanism in Marie Byrd Land related to a mantle plume? *Abstracts Sixth International Symposium on Antarctic Earth Sciences, 9–13 September 1991*. Tokyo: National Institute of Polar Resaerch, 337.

Lawver, L.A., Royer, J.-Y., Sandwell, D.T. & Scotese, C.R. 1991. Crustal development: Gondwana break-up, evolution of the Antarctic continental margins. *In* Thomson, M.R.A., Crame, J.A. & Thomson, J.W., eds. *Geological evolution of Antarctica*. Cambridge: Cambridge University Press, 533–540.

Leat, P.T. & Thompson, R.N. 1988. Miocene hydrovolcanism in NW Colorado, USA, fuelled by explosive mixing of basic magma and wet unconsolidated sediment. *Bulletin of Volcanology*, **50**, 229–243.

LeBas, M.J., LeMaitre, R.W., Streckeisen, A. & Zanettin, B. 1986. A chemical classification of volcanic rocks based on the total alkali-silica diagram. *Journal of Petrology*, **27**, 745–750.

LeMasurier, W.E. 1972a. Volcanic record of Antarctic glacial history: implications with regard to Cenozoic sea levels. *In* Price, R.J. & Sugden, D.E., *eds. Polar geomorphology, Special Publication 4*. London: Institute of British Geographers, 59–74.

LeMasurier, W.E. 1972b. Volcanic record of Cenozoic glacial history in Marie Byrd Land. *In* Adie, R.J., *ed. Antarctic geology and geophysics*. Oslo: Universitetsforlaget, 251–260.

LeMasurier, W.E. 1990a. Miocene-Oligocene centers, Mount Petras and USAS Escarpment. *Antarctic Research Series*, **48**, 239–243.

LeMasurier, W.E. 1990b. Marie Byrd Land. *Antarctic Research Series*, **48**, 146–163.

LeMasurier, W.E., Harwood, D.M. & Rex, D.C. 1994. Geology of Mount Murphy Volcano: an 8-m.y. history of interaction between a rift volcano and the West Antarctic ice sheet. *Geological Society of America Bulletin*, **106**, 265–280.

LeMasurier, W.E. & Landis, C.A. 1996. Mantle-plume activity recorded by low-relief erosion surfaces in West Antarctica and New Zealand. *Geological Society of America Bulletin*, **108**, 1450–1466.

LeMasurier, W.E., McIntosh, W.C. & Rex, D.C. 1981. Mid-Tertiary glacial history recorded at Mount Petras, Marie Byrd Land. *Antarctic Journal of the United States*, **16**(5), 19–21.

LeMasurier, W.E. & Rex, D.C. 1982. Volcanic record of Cenozoic glacial history in Marie Byrd Land and western Ellsworth Land: revised chronology and evaluation of tectonic factors. *In* Craddock, C., *ed. Antarctic geoscience*. Madison: University of Wisconsin Press, 725–734.

LeMasurier, W.E. & Rex, D.C. 1983. Rates of uplift and the scale of ice level instabilities recorded by volcanic rocks in Marie Byrd Land, West Antarctica. *In* Oliver, R.L., James, P.R. & Jago, J.B., *eds. Antarctic earth sciences*. Canberra: Australian Academy of Science, 660–673.

LeMasurier, W.E. & Wade, F.A. 1976. Volcanic history in Marie Byrd Land: implications with regard to southern hemisphere tectonic reconstructions. *In* Gonzalez-Ferran, O., *ed. Proceedings of the International Symposium on Andean and Antarctic Volcanology Problems*. Rome: IAVCEI, 398–424.

McPhie, J., Doyle, M. & Allen, R. 1993. *Volcanic textures: a guide to the interpretation of textures in volcanic rocks*. Hobart, TAS: Centre for Ore Deposit and Exploration Studies, University of Tasmania, 198 pp.

Samson, S.D. & Alexander, C.E. 1987. Calibration of the interlaboratory $^{40}Ar/^{39}Ar$ dating standard, Mmhb-1. *Isotope Geoscience*, **66**, 27–34.

Shackleton, N.J. & Kennett, J.P. 1975. Paleotemperature history of the Cainozoic and the initiation of Antarctic glaciation: oxygen and carbon isotope analyses in DSDP Sites 277, 279, and 281. *Initial Reports of the Deep Sea Drilling Project*, **29**, 743–755.

Skilling, I.P. 1994. Evolution of an englacial volcano: Brown Bluff, Antarctica. *Bulletin of Volcanology*, **56**, 573–591.

Smellie, J.L. & Hole, M.J. 1997. Products and processes in Pliocene-Recent, subaqueous to emergent volcanism in the Antarctic Peninsula: examples of englacial Surtseyan volcano construction. *Bulletin of Volcanology*, **59**, 628–646.

Smellie, J.L., Hole, M.J. & Nell, P.A.R. 1993. Late Miocene valley-confined subglacial volcanism in northern Alexander Island, Antarctic Peninsula. *Bulletin of Volcanology*, **55**, 273–288.

Smellie, J.L. & Skilling, I.P. 1994. Products of subglacial volcanic eruptions under different ice thicknesses: two examples from Antarctica. *Sedimentary Geology*, **91**, 115–129.

Sohn, Y.K. 1996. Hydrovolcanic processes forming basaltic tuff rings and cones on Cheju Island, Korea. *Geological Society of America Bulletin*, **108**, 1199–1211.

Sohn, Y.K. & Chough, S.K. 1992. The Ilchulbong tuff cone, Cheju Island, South, Korea: depositional processes and evolution of an emergent Sursetyan-type tuff cone. *Sedimentology*, **39**, 523–544.

Steiger, R.H. & Jaeger, E. 1977. Subcommission on geochronology: convention of the use of decay constants in geo- and cosmochronology. *Earth and Planetary Science Letters*, **36**, 359–362.

Thorarinsson, S., Einarsson, T., Sigvaldason, G. & Elisson, G. 1964. The submarine eruption off the Vestmann Islands 1963–1964: a preliminary report. *Bulletin of Volcanology*, **27**, 435–445.

Turner, G. & Cadogan, P.H. 1974. Possible effects of $^{39}Ar$ recoil in $^{40}Ar/^{39}Ar$ dating. *Geochimica et Cosmochimica Acta, Supplement 5*, **2**, 1601–1615.

Walker, G.P.L. & Croasdale, R. 1972. Characteristics of some basaltic pyroclastics. *Bulletin of Volcanology*, **35**, 303–317.

Waters, A.C. & Fisher, R.V. 1971. Base surges and their deposits: Capelinhos and Taal volcanoes. *Journal of Geophysical Research*, **76**, 5596–5614.

Wohletz, K. & Heiken, G. 1992. *Volcanology and geothermal energy*. Oxford: University of California Press, 432 pp.

Wohletz, K.H. 1983. Mechanisms of hydrovolcanic pyroclast formation: grain-size, scanning electron microscopy, and experimental studies. *Journal of Volcanology and Geothermal Research*, **16**, 31–63.

York, D. 1969. Least-squares fitting of a straight line. *Canadian Journal of Physics*, **44**, 320–324.